Available online at www.sciencedirect.com
SCIENCE DIRECT
Polymer 46 (2005) 8079–8090
polymer
www.elsevier.com/locate/polymer

Effect of microstructure of acrylic copolymer/terpolymer on the properties of silica based nanocomposites prepared by sol–gel technique

S. Patel, A. Bandyopadhyay, V. Vijayabaskar, Anil K. Bhowmick*

Rubber Technology Centre, Indian Institute of Technology, Kharagpur 721302, India

Received 24 February 2005; received in revised form 14 June 2005; accepted 24 June 2005
Available online 20 July 2005

Abstract

Acrylic copolymers/terpolymers with different comonomer contents were prepared by solution polymerization. Copolymers/terpolymers-silica hybrid composites were synthesized by acid catalyzed sol–gel technique using tetraethoxysilane (TEOS) as silica precursor. Microstructure of the copolymers and the terpolymers was analyzed by C^{13} nuclear magnetic resonance and Fourier transform infrared (FTIR) spectroscopy. The hybrid composites were characterized by scanning electron microscopy (SEM), FTIR, thermogravimetry, dynamic mechanical thermal analysis (DMTA) and their mechanical properties. The results showed that an increase in hydrophilicity of the polymer matrix and the ratio of ethyl to butyl acrylate, and incorporation of acrylic acid as termonomer helped in finer dispersion of silica and prevented macrophase separation. There was no evidence of chemical interaction between the polymer and the dispersed silica phase. Dynamic mechanical thermal analysis indicated mechanical reinforcement within the hybrid composites. As a result, these composites demonstrated superior tensile strength and tensile modulus with increasing proportion of TEOS up to a certain level. At a particular TEOS concentration, the tensile properties improved with increasing hydrophilicity of the polymer matrix and acrylic acid modification. The mechanism for improvement in mechanical and dynamic mechanical properties of the hybrids was discussed.

Keywords: Acrylic copolymers and terpolymers; Nanocomposites; Sol–gel

1. Introduction

Organic/inorganic hybrid nanocomposites has been of great interest in recent years, since these offer combined properties of organic polymers (flexibility and low density) and inorganic materials (rigidity, hardness and thermal stability) and also acquire some special properties like higher reinforcement [1], optical transparency [2], flame retardancy [3], decreased gas permeability [4], electrical [5] and magnetic [6] properties. There are several ways of synthesizing these nanocomposites. Among them, the sol–gel technique has become popular because of its mild processing condition [2,10,11]. Typical sol–gel process includes two steps, namely hydrolysis and condensation as exemplified by alkoxysilane as shown in Scheme 1 [2,10,11].

Initially, an alkoxysilane undergoes catalytic hydrolysis and then subsequently condenses to generate silica particles. In most of the cases, tetraethoxysilane (TEOS) has been used for this purpose. The relative kinetics of each step can affect the morphology of the in situ generated silica particles. During hydrolysis and condensation of TEOS under basic conditions, the rate of condensation is faster relative to the hydrolysis rate, resulting in a denser cluster growth leading to particulate-like structures [10]. In contrast, if the hydrolysis and condensation reactions are carried out in the presence of an acid more linear or polymer-like chain structures are formed, due to higher hydrolysis rate compared to the condensation rate [10]. Besides the nature of the catalysts used, pH has a dramatic effect on the reaction rate and hence on the morphology of the resulting silica network. Interaction of polymer with silica particles also plays an important role. Polymer having functional groups that have specific interactions with silanol groups of in situ generated silica by sol–gel reaction can prevent the macro phase separation and can result in composites with high homogeneity and optical transparency [7–9,11].

* Corresponding author. Tel.: +91 3222 283180; fax: +91 3222 220312.
E-mail address: anilkb@rtc.iitkgp.ernet.in (A.K. Bhowmick).

0032-3861/$ - see front matter © 2005 Elsevier Ltd. All rights reserved.
doi:10.1016/j.polymer.2005.06.067

Hydrolysis

$$Si(OR)_4 + nH_2O \xrightarrow{H^+ / OH^-} (RO)_{4-n}Si(OH)_n + n\ ROH$$

Condensation

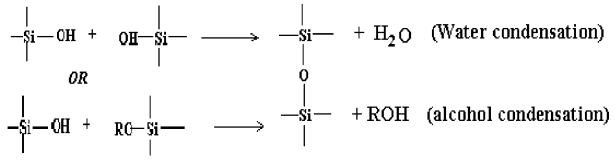

where R is an alkyl group.

Scheme 1.

There have been many hybrid polymer composites containing nano silica prepared by the sol–gel approach, which have focused on the influence of nano particles on mechanical, thermal and optical properties of the composites [2,12–18]. Recently, Bandyopadhyay et al. [2,12] have reported a number of rubber/silica hybrid nanocomposites by sol–gel technique from this laboratory. Till now the authors are not aware of any published report on the effect of copolymer/terpolymer composition on the properties of nanocomposites, which has been the subject of our current investigation. The copolymers and the terpolymers synthesized are based on ethyl acrylate (EA), butyl acrylate (BA), and acrylic acid (AA). The nanocomposites have been prepared by using sol–gel reaction with TEOS under acid catalysis.

2. Experimental

2.1. Materials

Tetraethoxysilane (TEOS, density = 930 kg/m^3, boiling point 168 °C) was procured from Acros Organics (USA). Ethyl acrylate (EA) was supplied by Burgoyne Burbidges&Co. (India). Butyl acrylate (BA) and acrylic acid (AA) were supplied by Loba Chemie Pvt. Ltd, Mumbai (India). Benzoyl peroxide (BPO, 97% purity) was purchased from Aldrich Chemicals (USA). Hexamethylethelenediamine carbamate (HMDC, DIAK#1) was generously supplied by NICCO Corp. Ltd (India). Tetrahydrofuran (THF, 99% pure) and benzene were procured from Merck Ltd (India). Sodium hydroxide, deionized water and concentrated hydrochloric acid, all of laboratory grade, were obtained from indigenous sources.

2.2. Synthesis of acrylic copolymers and terpolymers

EA and BA were made inhibitor-free by repeated washing with 4% aqueous NaOH solution and then by vacuum distillation. AA was also purified by vacuum distillation. Acrylic copolymers/terpolymers with varying monomer contents were synthesized by well-known solution polymerization technique in benzene using BPO as initiator. The comonomer contents were adjusted by calculating the T_g of the copolymers (Table 1) from the Fox equation.

$$\frac{1}{T_g} = \frac{W_1}{T_{g1}} + \frac{W_2}{T_{g2}}$$

Where T_g, glass transition temperature for copolymer (K); T_{g1}, glass transition temperature for comonomer 1 (K); T_{g2}, glass transition temperature of comonomer 2 (K); W_1, weight fraction of comonomer 1; W_2, weight fraction of comonomer 2.

Polymerization was carried out in an inert atmosphere of nitrogen at 70 °C. 50 g of benzene as a solvent was taken in the reactor. BPO as initiator (0.06 wt%) was dissolved in 75 g of the monomers and the mixture was added drop wise to the to the reactor for initial 2 h followed by further 2 h reaction with a continuous stirring condition. The reaction was stopped at 82% monomer to polymer conversion. Table 1 reports in detail the composition of the copolymers and terpolymers synthesized for this study. Intrinsic viscosity of all copolymers and terpolymers was determined by Ostwald viscometer (Table 1). Microstructure of the polymers was analyzed by nuclear magnetic resonance (NMR) spectroscopy and infrared (FTIR) spectroscopy, the details of which are given later.

Table 1
Theoretical composition of copolymers/terpolymers

Copolymer/terpolymer designation	Theoretical[a] EA (wt%)	Theoretical[a] BA (wt%)	Theoretical[a] AA (wt%)	Intrinsic viscosity (dl/g)	T_g[b] (°C)
50E	50	50	–	2.24	−36
75E	75	25	–	2.26	−29
85E	85	15	–	2.27	−25
1A85E	85	15	1	2.32	–
3A85E	85	15	3	2.30	–
5A85E	85	15	5	2.34	–

[a] The theoretical acrylic acid variation is done to modify the copolymer backbone. The T_g of these resultant terpolymers cannot be calculated theoretically using the Fox equation and are therefore not reported.
[b] Calculated from the Fox equation.

2.3. Preparation of hybrid composites by sol–gel technique

A 20% solution was prepared by dissolving desired amount of the copolymer/terpolymer in THF. The pH of the solution was adjusted to 1.0–2.0 by adding appropriate amount of concentrated HCl, which also acts as the catalyst for the sol–gel reaction. TEOS and deionized water in the molar ratio of 1:2 [2,12] were thoroughly mixed by vigorous stirring for 5 min and then added to the polymer solution, under stirring conditions at ambient temperature. The precursor solution for preparing hybrid composites was stirred for 30 min at room temperature and then poured over a uniform and thoroughly cleaned glass plate for gelation. The initial evaporation of solvent was carried out under controlled conditions for 24 h. In the next phase, further evaporation for 5 days was allowed to remove the residual solvents and by products of sol–gel reaction (water and ethanol). The optimum gelling time was taken as the time when practically no weight variation of the hybrid composite was observed. The proportion of TEOS was varied from 0 to 50 wt% in all the copolymers and the terpolymers, as listed in Table 2. Since these copolymers/terpolymers were rubbery in nature ($T_g <$ ambient temperature), crosslinking reaction was carried out by dispersing HMDC in the resultant polymer. Addition of curative was made only after complete mixing of TEOS and water in the acidified polymer solutions for 30 min. The curative was mixed for further 1 h at ambient temperature. The films were cast over plane glass plate as before and gelled to constant weight. Curing of the film was done in an air oven at 170 °C for 30 min followed by 24 h post curing at 70 °C. Curing conditions were optimized by measuring the gel content of the resultant samples. The details of the sample compositions and their designations used in this study are listed in Table 2.

Table 2
Compositions of hybrid composites

Sample designation	TEOS (wt%)	HMDC (wt%)	Appearance of the films
50E	–	–	Transparent
50EN30	30	–	Opaque
50EN30	50	–	Opaque
75E	–	–	Transparent
75EN30	30	–	Opaque
75EN50	50	–	Opaque
85E	–	–	Transparent
85EN10	10	–	Transparent
85EN20	20	–	Transparent
85EN30	30	–	Transparent
85EN40	40	–	Translucent
85EN50	50	–	Translucent
1A85E	–	–	Transparent
1A85EN10	10	–	Transparent
1A85EN20	20	–	Transparent
1A85EN30	30	–	Transparent
1A85EN40	40	–	Translucent
1A85EN50	50	–	Translucent
3A85E	–	–	Transparent
3A85EN30	30	–	Transparent
3A85EN50	50	–	Transparent
5A85E	–	–	Transparent
5A85EN30	30	–	Transparent
5A85EN50	50	–	Transparent
85EX	–	2.5	Translucent
85EN30X	30	2.5	Translucent
85EN50X	50	2.5	Translucent
1A85EX	–	2.5	Translucent
1A85EN10X	10	2.5	Translucent
1A85EN30X	30	2.5	Translucent
1A85EN50X	50	2.5	Translucent
3A85EX	–	2.5	Translucent
3A85EN30X	30	2.5	Translucent
3A85EN50X	50	2.5	Translucent
5A85EX	–	2.5	Translucent
5A85EN30X	30	2.5	Translucent
5A85EN50X	50	2.5	Translucent

2.4. Characterization of pure copolymer and terpolymer and their hybrid composites

2.4.1. Infrared (IR) spectroscopy

The infrared (IR) spectra of the control polymer and the hybrid composites films were recorded with a Nicolet Nexus Fourier transform infrared spectrometer (FTIR) in ATR mode by using 45° KRS5 prism at room temperature. The samples were scanned from 4000 to 600 cm^{-1} with a resolution of 4 cm^{-1}. All the spectra were taken after an average of 32 scans for each specimen.

2.4.2. Solid state nuclear magnetic resonance (NMR) spectroscopy

The solid state C-13 Fourier transform nuclear magnetic resonance (FTNMR) experiments were performed at 75.5 MHz on a Bruker 300MSL spectrometer. Magic angle spinning (MAS) and high power proton decoupling were used with cross polarization (CP) to obtain the spectra. The spinning speeds ranged from 1.0 to 3.0 kHz at 70 °C. The spectral width was 29,240 Hz and 512 data points with acquisition time of 0.014 s were collected for each spectrum.

2.4.3. Scanning electron microscopy (SEM) and energy dispersive X-ray (EDX) silicon mapping

The dispersion of silica particles in the polymer matrices was observed through microscopic investigations with a JEOL JSM 5800 scanning electron microscope. The samples were sputter coated with gold to avoid the artifacts associated with sample charging. All the images were taken with the acceleration voltage of 20 kV. The X-ray silicon mapping of the hybrid composite films was recorded in an Oxford EDAX system, attached to the microscope.

2.4.4. Determination of mechanical properties

The mechanical properties of the hybrid composites were determined by a Universal Testing Machine (UTM, Zwick 1445) on tensile dumbbell specimens, punched out from the

cast films by using ASTM Die C. The tests were carried out as per ASTM D 412-99 method at ambient temperature with grip separation speed of 500 mm/min. The average value of three tests is reported for each sample.

2.4.5. Dynamic mechanical thermal analysis (DMTA)

Dynamic mechanical thermal characteristics of the hybrid composite films were evaluated by a DMTA IV (RHEOMETRIC SCIENTIFIC) under tension mode. The experiments were carried out at a frequency of 1 Hz. The measurements were taken from −70 to 70 °C at a heating rate of 2 °C/min. The data were analyzed by using RSI Orchestrator application software on an ACER computer attached to the machine. The storage modulus and loss tangent (tan δ) were measured for all the samples under identical conditions.

2.4.6. Heat aging test

Accelerated heat aging test of the cured samples was performed as per ASTM D573 method in an air oven at 100 °C for 24, 48, and 72 h. Then the mechanical properties were studied as per ASTM D 412-99 method at ambient temperature with grip separation speed of 500 mm/min before and after aging. Average value of three tests is reported for each sample.

2.4.7. Thermogravimetric analysis (TGA)

Themogravimetric analysis of the hybrid composites was performed by using a DuPont TGA instrument (Model no. 2000) from ambient temperature to 800 °C at a programmed heating rate of 20 °C/min in nitrogen atmosphere. A sample weight of ~10 mg was taken for all the measurements. The weight loss against temperature was recorded.

3. Results and discussion

3.1. Characterization of the copolymer and the terpolymer

3.1.1. Infrared spectroscopic (FTIR) analysis

The FTIR spectra of different polymers are shown in Fig. 1. The characteristic peaks are assigned in Table 3. The strong absorption bands at 1720–1730 and 1153 cm^{-1} corresponding to carbonyl (>C=O) stretching and asymmetric C–O–C stretching are found to be present in all the polymers. In the terpolymers, differentiation between ester

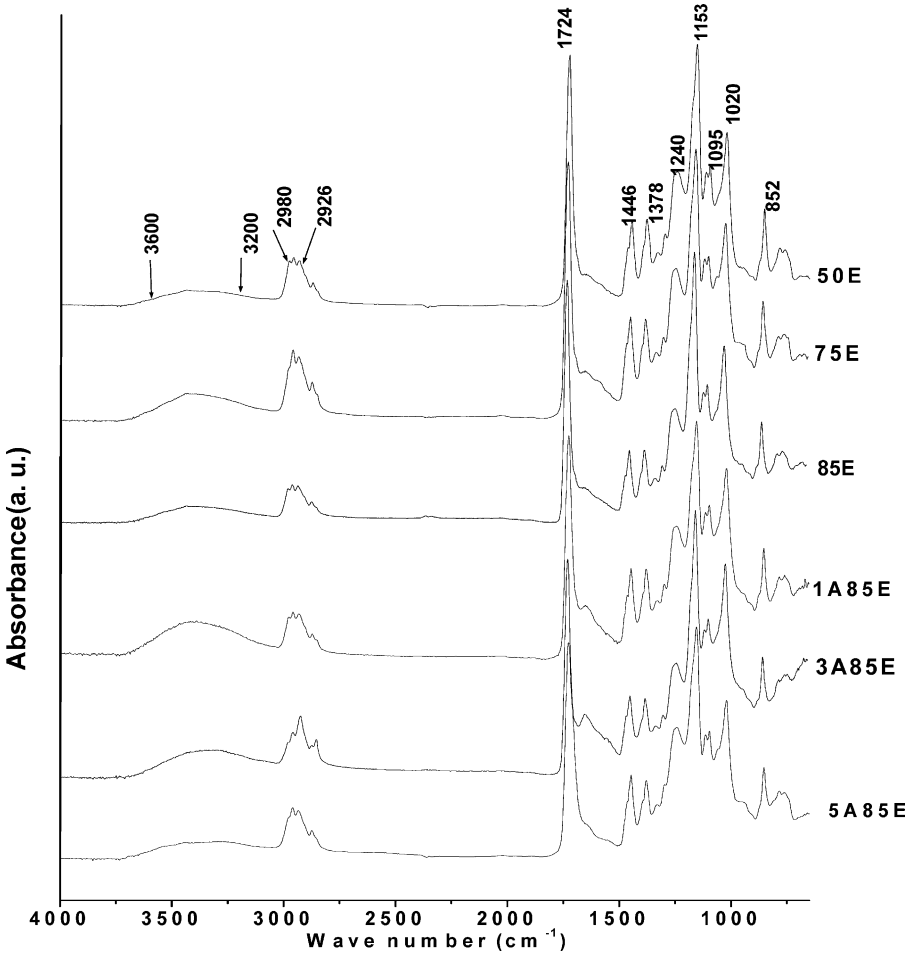

Fig. 1. FTIR spectra of all pure polymers.

Table 3
FTIR peak assignments for pure polymers and hybrid composites

Wave number (cm^{-1})	Functional group
3600–3200	–OH stretching of acrylic acid, –OH stretching of water
2960	Asymmetric $–CH_3$ stretching of $O–CH_2CH_3$
2935	$–CH_3$ stretching of $O–CH_3CH_3$
1724	>C=O stretching
1446	–C–H bending
1378	–C–H deformation
1240, 1153	Asymmetric C–O–C stretching vibration of acrylates
1020, 1095	Skeletal vibration, Si–O–Si stretching, asymmetric Si–O–C stretching
939	Si–O stretch of silanol
852	C–O–C deformation, symmetric Si–O–C stretching

>C=O and acid >C=O could not be made since both the peaks merge to exhibit single band at 1724 cm^{-1}. Absorption band due to O–H stretching of acrylic acid, which usually occurs in the region of 3000–3200 cm^{-1}, becomes much broader (3100–3650 cm^{-1}) because of absorbed moisture in the sample. It seems that all the samples contain this stretch. Absorption bands due to C–H bending, C–H deformation and CH_3 stretching vibration of $O–C_2H_5$ appear at 1446, 1378 and 2960 cm^{-1}, respectively. Absorption bands at 1153 and 1240 cm^{-1} are due to the presence of symmetric C–O–C and asymmetric C–O–C stretching vibrations of acrylates. Absorption band due to skeletal vibration of acrylates is observed in the range of 1020–1095 cm^{-1} in all the samples. An associated peak of C–O–C deformation is also observed at 851 cm^{-1}.

3.1.2. Solid state nuclear magnetic resonance (NMR) spectroscopic analysis

The C-13 solid state NMR spectra of the terpolymer of EA and BA and AA in the ratio of 85:15:3 and the copolymer of EA and BA in the ratio of 85:15 were taken. The spectrum of the terpolymer recorded at 70 °C is shown in Fig. 2. It is clear that the peaks are sharper for these samples and line broadening is avoided (Fig. 2). This indicates that ^{13}C spin relaxation times of those carbons in that ppm range are short at higher temperature and this condition is sufficient for accurate quantification of different peaks. This concept of ^{13}C solid state NMR spectra at higher temperature has been reported by Hill et al. [19]. Characteristic peak corresponding to carboxylic group of acrylic acid is observed at 173 ppm in the terpolymer. It is difficult to distinguish between the ester and carboxylic peaks. Peaks at 175.3 and 176.2 ppm are observed with low intensities for the ester groups of BA and EA, respectively. A peak is found at 14.1 ppm which corresponds to $–CH_3$ group of ester present in BA. Several peaks are found in the aliphatic region of 20–60 ppm. This will correspond to $–CH_2–$ and –CH– linkages due to a particular sequence distribution. An attempt has been made to study the sequence of the two monomers distributed in the polymer chain. This involves the assumption of various sequences such as HTHT, HHTT, HTTH, HHHH, TTTT, HTTT and HHHT, respectively, where H stands for head and T for tail. As an example, the structures of HHTT and HTHT are shown in Fig. 3. The theoretical carbon resonances are calculated as per additivity principle and compared with the values in the Sadtler guide. Peaks at 26.2 and 33.1 ppm corresponding to $–CH_2$ groups and at 61.3 and 44.3 ppm for –CH groups in HHTT structure are observed in both the cases. The copolymer and the terpolymer have an arrangement of poly(ethyl acrylate) in HHTT sequence separated by BA units. Special attention has also been given to determine the molecular composition of EA and BA in the acrylic copolymer. A procedure by Martino and Kelchtermans [20] is adopted. In all the methods [20], the

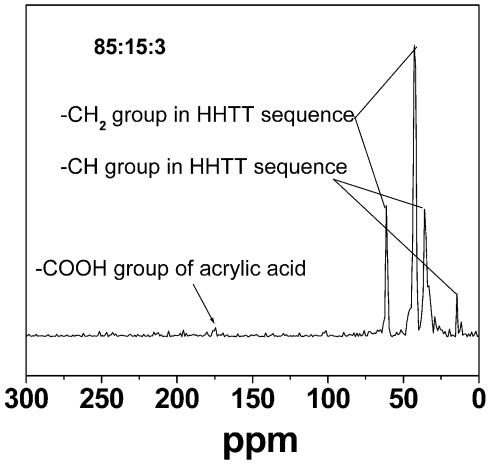

Fig. 2. NMR spectra of 85:15:3 (EA:BA:AA) terpolymer.

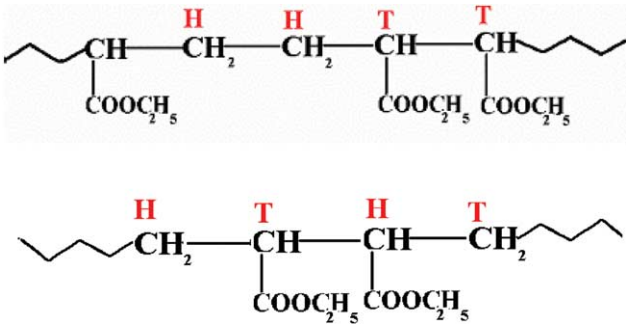

Fig. 3. HHTT and HTHT sequence distribution of monomer.

integral areas in C-13 spectra are combined in various ways to determine the monomer concentrations. In this procedure mentioned below, all the carbons in the spectra are used.

$$\text{Mol\% of ethyl acrylate} = \frac{(S_c + T_c + U_c - 2V_c)}{(S_c + T_c + U_c)} \times 100$$

$$\text{Mol\% of butyl acrylate} = 100 - \text{Mol\% of ethyl acrylate}$$

S_c, all secondary carbons; T_c, all tertiary carbons; U_c, ester carbonyl in acrylate; V_c, methylene carbons in butyl acrylate.

This method revealed that the EA and BA are in the ratio 81.8:18.2 in the HHTT copolymer sequence.

3.2. Characterization of the hybrid composites

3.2.1. Microscopic observations

The SEM micrographs of the representative hybrid composites prepared from 50E, 75E, 85E, 1A85E and 5A85E are compared in Fig. 4(a)–(f). SEM pictures of 50EN50 and 75EN50 in Fig. 4(a) and (b) show agglomeration of silica with particles size ranging from 1 μm–500 nm (average 400 nm) and 550–100 nm (average 180 nm) respectively. In contrast, the SEM micrograph of 85EN10 in Fig. 4(c) shows fine dispersion of silica particles with an average size of 15 nm. When the concentration of TEOS is increased to 50 wt% in the same matrix, the average size of these silica particles increases up to 120 nm with few local agglomerations (Fig. 4(d)). This discrimination is probably

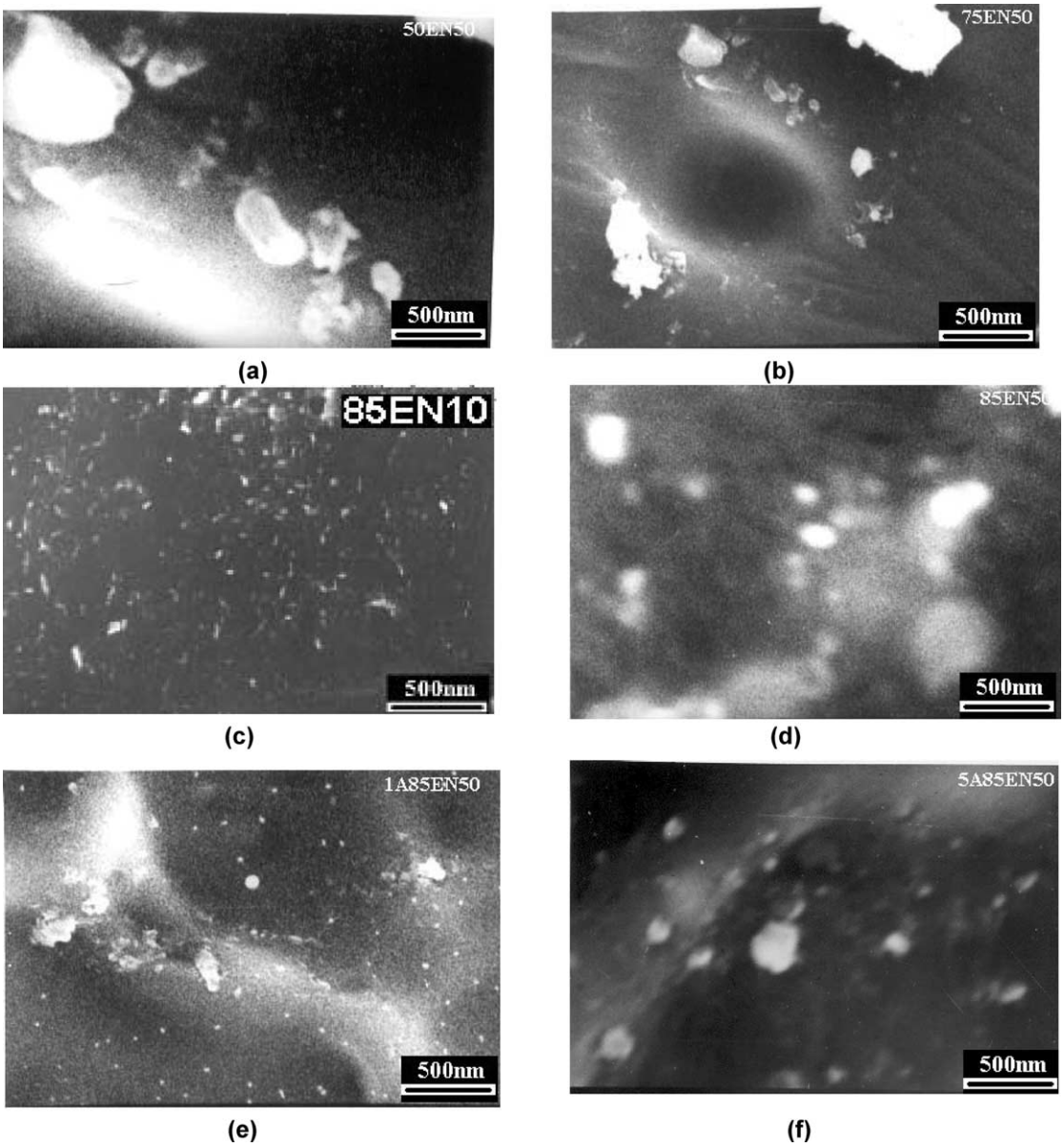

Fig. 4. SEM micrographs of hybrid composites. (a) 50EN50 (b) 75EN50 (c) 85EN10 (d) 85EN50 (e) 1A85EN50 (f) 5A85EN50.

due to the increased polarity (hydrophilicity) in 85E polymer matrix, due to higher EA content, which facilitates the dispersion of the inorganic silica phase. Similar observation is obtained with 5A85EN50 hybrid composite (Fig. 4(f)). In this case, silica particles are even finely distributed (average particle size 80 nm) and also the extent of aggregation is reduced from that of 85EN50. This observation could be explained on the basis of further improvement in the polarity of the matrix 85E by the incorporation of acrylic acid (5 wt%). This increase in polarity increases the interaction at the organic–inorganic interfaces, which was not the case in 50EN50 and 75EN50, shown earlier.

Dispersion and aggregation phenomenon of silica within polymer matrixes is further confirmed through the EDX study of the hybrid composites, displayed in Fig. 5(a)–(c). The white spots over the dark background indicate the location of silicon within the hybrid composites. Fig. 5(a) and (b) corresponding to the hybrid composites, 50EN50 and 85EN50 show uniform distribution of silicon along with few aggregations, keeping parity with their SEM pictures. Uniform dispersion of white spots in Fig. 5(c) reveals much better dispersion of silica in 1A85EN50. This dispersion behavior of silica phase has affected the visual appearance of the hybrid composites. The composites containing silica particles predominantly as a finely dispersed phase is transparent, while the composites having aggregated silica particles as the major inorganic phase are opaque (Table 2).

3.2.2. Infrared spectroscopic (FTIR) analysis

The FTIR spectra of the representative uncured hybrid composites, each containing 30 wt% TEOS, are compared in Fig. 6. The characteristic peaks are assigned in Table 3. Interestingly, the band position of the ⟩C=O stretches in hybrid composites remain unchanged from that of the control samples. This indicates that the interaction between the organic and the inorganic phases is not through stronger chemical bonding but only by means of weak dipolar interaction. Infact, this observation is similar to the one inferred in the case of commercial acrylic rubber/silica hybrid composites reported from our laboratory [2]. The absorption due to Si–O–Si asymmetric stretches for silica in all the hybrid composites is likely to be merged with the skeletal vibration of acrylates. But the appearance of peaks

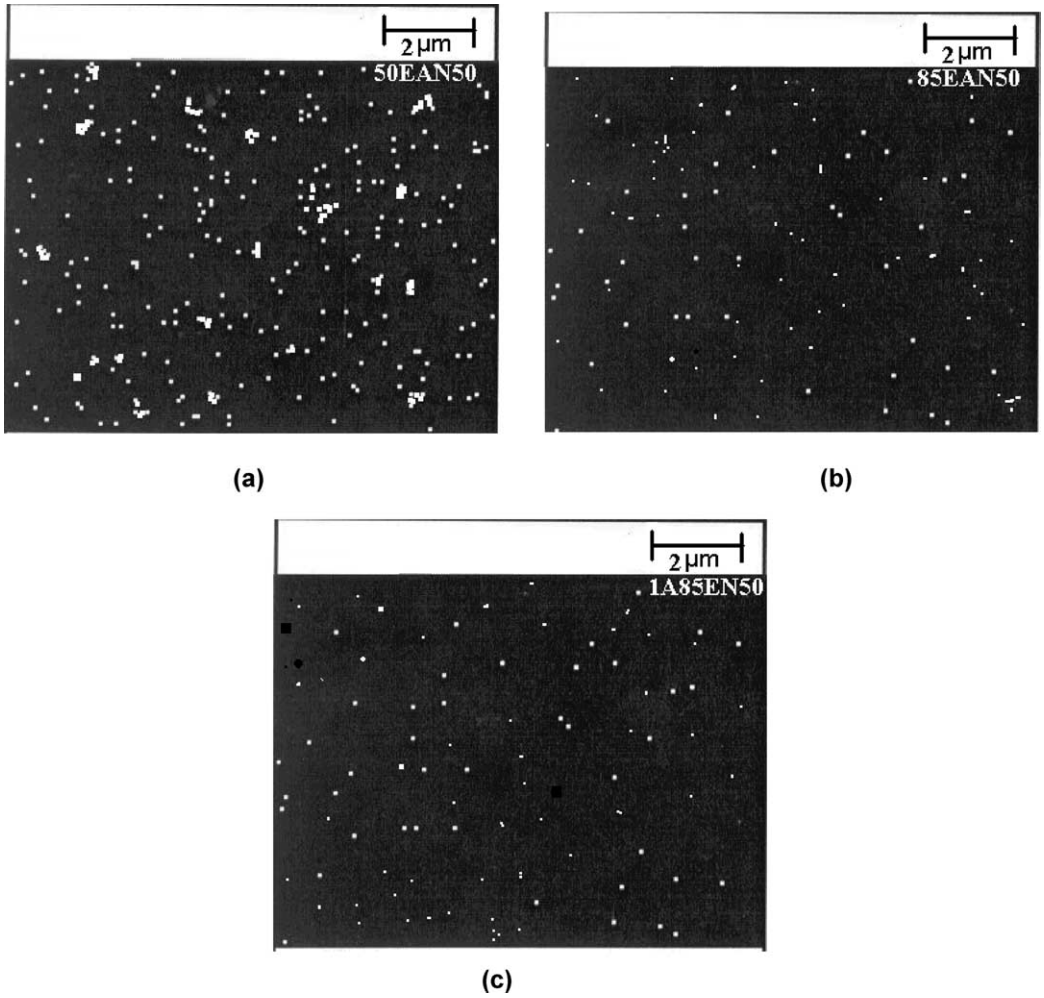

Fig. 5. X-ray silicon mapping of hybrid composites (a) 50AN50 (b) 75EN50 (c) 5A85EN50.

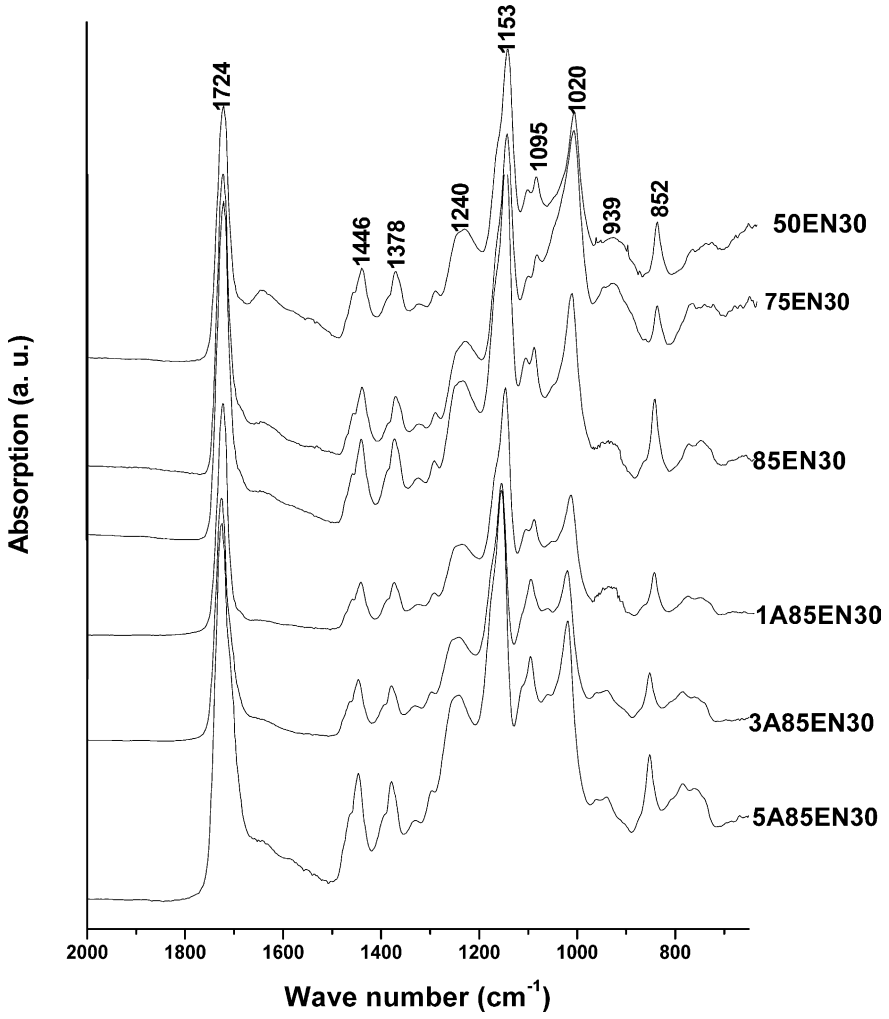

Fig. 6. FTIR spectra of representative hybrid composites.

at 1095 and 1020 cm^{-1} in 50EN30 indicates the presence of different siloxane structure composed of ring and linear chain type configuration. As the polarity of the matrix polymer is increased, the peak at higher energy (1095 cm^{-1}) converts to shoulder, whereas the peak at lower energy (1020 cm^{-1}) remains prominent (Fig. 6). Nevertheless, a shoulder is observed in the region of 950–920 cm^{-1} in the hybrid composites, elucidating the presence of silanol groups (Si–OH) in the samples, resulting from the incomplete condensation reaction. In order to explain the effect of different microstructures in the hybrid composites, the normalized peak absorption ratio corresponding to Si–O–Si asymmetric stretching (1095 and 1020 cm^{-1}) and silanol stretching (950 cm^{-1}) to constant peak absorption of C–H bending (1446 cm^{-1}) against polymer compositions is separately plotted in Fig. 7(a) and (b). In both the copolymer and the terpolymer hybrid composites the absorption at 1020 cm^{-1} shows steady decrease with increase in matrix polarity. On the other hand, the absorption at 1095 cm^{-1} registers an increase from 50E to 85E in the copolymer hybrid composites, while this increase is sharper for the composite 3A85E and 5A85E, as evident from Fig. 7(a) and (b). The absorption in the 930–950 cm^{-1} region due to Si–OH stretching shows steady increase. From this observation, it is clear that when the polarity of the matrix increases, definite changes in the microstructure of the silica occur. Substantial increment in the Si–OH absorption with increasing matrix polarity indicates existence of more free silanol groups in the inorganic phase. This may be ascribed to favorable interaction with the polymer backbone. This phenomenon has played the key role for finer dispersion of the silica particles in the AA modified composites compared to 85E sample. This is clear from the SEM micrographs in Section 3.2.1.

3.2.3. Mechanical properties

The tensile stress–strain plots for representative hybrids containing 50 wt% TEOS in cured and uncured states are compared in Fig. 8(a) and (b). The tensile strength (maximum tensile stress in the case of the uncured samples), modulus (at 50 and 300%) and elongation at break (%) values for all the samples are listed in Tables 4 and 5. The

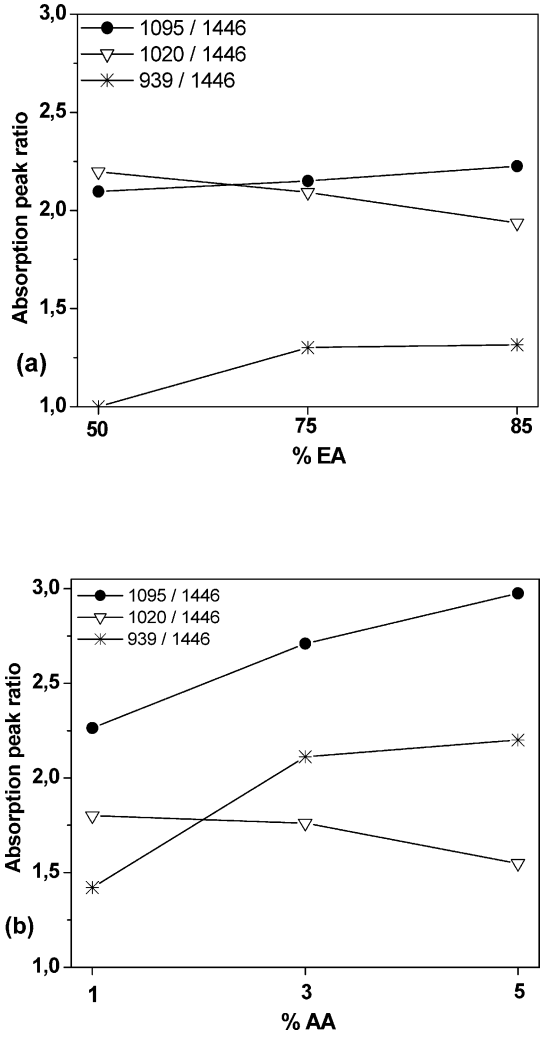

Fig. 7. Effect of microstructure on Si–O stretching of silanol and Si–O–Si stretching (a) In copolymer hybrid composites (b) In terpolymer hybrid composites.

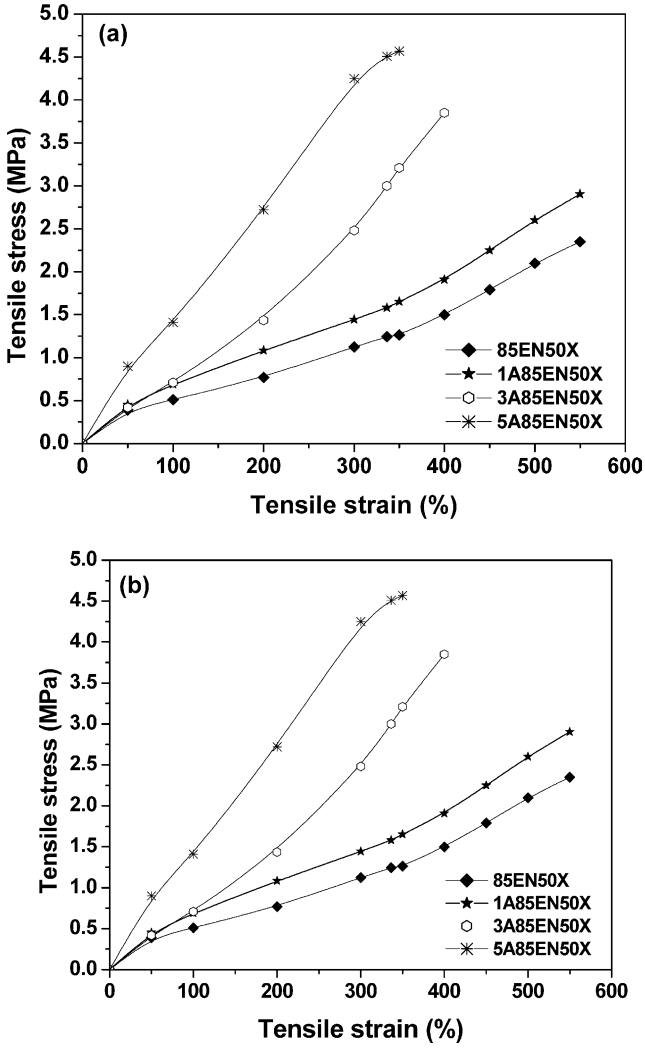

Fig. 8. (a) Effect of polymer microstructure on stress–strain properties of uncured hybrid composites; (b) effect of polymer microstructure on stress–strain properties of cured hybrid composites.

strength of the composites increases when TEOS is added, but this increase is more in the case of 85EN50 (81%) as compared to 50EN50 (66%). This is due to finer dispersion of in situ silica particles at highest EA concentration (85%) in the copolymer, as seen in the micrographs. The strength further increases in the acrylic acid modified terpolymers, which is again ascribed to finer dispersion of silica particles. On addition of acrylic acid (refer to SEM pictures in Fig. 4), smaller silica particles provide higher surface to volume ratio for interaction with the matrix. Moreover, higher silanol concentration in these particles also adds to this phenomenon. All these uncured hybrid composites exhibit very high elongation (>900%).

On crosslinking the hybrid composites based on 85E, the strength further increases. There is a similar trend observed in the case of the uncured hybrid composites, i.e. with increasing polarity (higher AA content) this improvement is higher (520 and 190% increase in tensile strength and modulus at 50% in 5A85EN50 compared to 81 and 107% in 85EN50). On the other hand, the elongation at break (%) values gradually decreases with increasing strength of the crosslinked hybrid composites. The results are explained on the basis of crosslinking of the acrylic matrices and nanosilica reinforcement within the crosslinked samples.

Table 6 represents the retention in mechanical properties of the 1% AA modified terpolymer nanocomposites containing 30 and 50 wt% TEOS after ageing at 100 °C for different time intervals (24, 48 and 72 h). The nanocomposites display better resistance towards oxidation compared to the control sample. This result may be due to the dispersion of nanosilica particles within the polymer matrix, which act as heat sinks. Slight increase in modulus and the decrease in elongation at break (%) values indicate that the nanocomposites are brittle on aging. The oxidative stability is improved on increasing the TEOS concentration, which is quite expected, due to generation of higher amount of silica particles.

Table 4
Mechanical properties of uncured samples

Sample designation	Maximum strength (MPa)	Elongation at break (%)	Modulus at 50% (Mpa)
50E	0.12	>900	0.11
50EN30	0.18	>900	0.17
50EN50	0.20	>900	0.19
75E	0.16	>900	0.15
75EN30	0.23	>900	0.21
75EN50	0.26	>900	0.24
85E	0.16	>900	0.13
85EN10	0.22	>900	0.20
85EN20	0.23	>900	0.21
85EN30	0.25	>900	0.22
85EN40	0.27	>900	0.25
85EN50	0.29	>900	0.27
1A85E	0.17	>900	0.15
1A85EN10	0.29	>900	0.20
1A85EN20	0.29	>900	0.21
1A85EN30	0.33	>900	0.23
1A85EN40	0.36	>900	0.27
1A85EN50	0.41	>900	0.29
3A85E	0.40	>900	0.31
3A85EN30	0.85	>900	0.54
1A85E5N0	1.05	>900	0.76
5A85E	0.53	>900	0.31
5A85EN30	2.80	>900	0.67
5A85EN50	3.29	>900	0.90

3.2.4. Dynamic mechanical thermal analysis (DMTA)

Fig. 9(a) and (b) shows the plots of dynamic storage modulus (log scale) and tan δ of the representative cured hybrid nanocomposites based on 85E and 5% acrylic acid modified 85E. The experimental temperature ranges from −70 to +70 °C. Viscoelastic response of these nanocomposites (85EN50, 5A85EN30 and 5A85EN50) is a direct evidence of the interaction of the nanosilica with the respective copolymers and terpolymers. The storage modulus vs. temperature plots in Fig. 9(a) shows that the modulus of all the samples in the glassy region is almost the same, but in the transition and the rubbery regions, the difference in moduli is significant. With the addition of 50% TEOS in 85E, the nanocomposite (85EN50) shows distinctly higher modulus, whereas the modulus further increases when 85E (A) matrix is modified with 5% AA (5A85E). This is ascribed to the greater polymer–silica interaction and higher interchain interaction in 5A85E due to the presence of AA. Drastic increment in modulus is noticed when TEOS is added to 5A85E matrix. The modulus, which starts dropping at around −30 °C for C (5A85EX), shifts to around −10 °C (+20 °C shift) for D (5A85EN30, 30 wt% TEOS) and E (5A85EN50, 50 wt% TEOS). Significant increase in the modulus of D and E (especially E, as it contains similar TEOS concentration) from that of B is due to the finer silica structures in the former compared to the later, as reported in Section 3.2.3. In the rubbery region, however, the nanocomposites with higher TEOS concentrations show higher modulus. Interestingly in the rubbery region, the compositions—B, D and E are superior to the compositions A and C due to the presence of silica. This is significant, as 'C' shows higher modulus than B in the transition region.

Significant changes in the viscous loss characteristics of the hybrid nanocomposites are visible from the tan δ vs. temperatures plots in Fig. 9(b). There is about 20% decrease in tan δ peak height (tan δ_{max}) from A to B due to the presence of nanosilica and their interaction. On the other hand, tan δ_{max} further decreases by 40% (and the peak marginally broadens) when 85E is modified with 5% AA. The T_g of A is −29 °C, which changes to −25 °C in B and −22 °C in C. Decrease in tan δ_{max} as well as broadening of tan δ peak indicates restricted movement of the polymer chains due to interaction. In B, this interaction is between the nanosilica and the polymer, whereas in C it is either inter or intra chain type. For D and E, tan δ_{max} shows drastic shift to the higher value (T_gs for D and E are −1 and +3 °C, respectively) as well as the peak broadens from that of the sample C. (although the tan δ_{max} for C and D are almost the same). This is again due to greater polymer–filler interaction in D and E, when the silica particles are finer.

Table 5
Mechanical properties of cured samples

Sample designation	Tensile strength (MPa)	Elongation at break (%)	Modulus at 50% (Mpa)	Modulus at 300% (Mpa)
85EX	0.54	600	0.30	0.50
85EN30X	1.88	540	0.37	0.92
85EN50X	2.35	550	0.39	1.16
1A85EX	0.55	655	0.30	0.50
1A85EN30X	2.44	650	0.40	1.05
1A85EN50X	3.05	550	0.45	1.44
3A85EX	1.17	319	0.23	0.61
3A85EN30X	3.30	544	0.35	1.60
3A85EN50X	3.85	392	0.42	2.48
5A58EX	1.34	455	0.29	1.11
5A85EN30X	3.73	333	0.71	3.32
5A85EN50X	4.57	330	0.90	4.25

Table 6
Results of heat ageing in an air oven at 100 °C

Sample designation	Ageing time (h)	Change in elongation at break (%)	Change in tensile strength (%)	Change in 300% modulus (%)
1A85EX	0	–	–	–
	24	0	−20	−36
	48	0	−35	−36
	72	0	−46	−52
1A85EN30X	0	–	–	–
	24	−29	−14	+14
	48	−40	−23	+39
	72	−44	−42	−7
1A85EN50X	0	–	–	–
	24	14	−7	+12
	48	−27	−14	+8
	72	−34	−31	−9

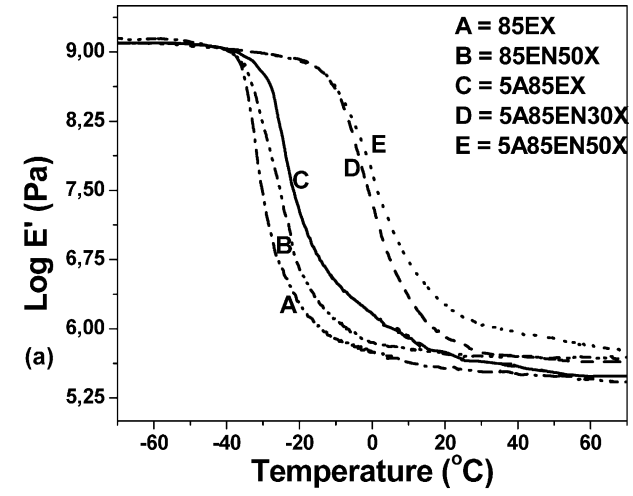

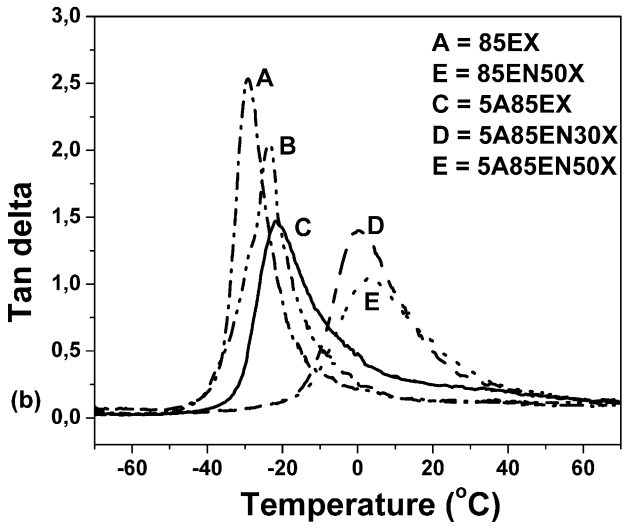

Fig. 9. (a) Storage modulus vs. temperature plots for representative crosslinked hybrids composites; (b) tan δ vs. temperature plots for representative crosslinked hybrids composites.

3.2.5. Themogravimetric analysis

The best mechanical properties are obtained with acrylic acid modified samples; hence they are further considered for thermal degradation studies. Fig. 10(a) and (b) shows the TGA and DTG thermograms of the crosslinked representative 1% AA modified terpolymer hybrid composites with different TEOS concentrations (10, 30 and 50 wt%). The thermal degradation temperature corresponding to initial 10% weight loss is almost same for pure 1A85EX and 1A85EN10X hybrid composites (Table 7). It is probably due to lack of any chemical interaction between the organic and the inorganic phase in the hybrid composites. The 30 wt% TEOS and 50 wt% TEOS loaded hybrid composites show more initial weight loss before 150 °C as compared to 1A85EX and 1A85EN10X, which is due to the presence of moisture in the samples. The peak degradation temperature, as traced from the DTG curves (Fig. 10(b)) and reported in Table 7, also does not shift to higher temperature for these composites. In contrast, the rate of degradation is considerably improved in the hybrid composites, as evident from the lowering of the peak height in DTG curves. Actually, the peak height gradually decreases on increasing the TEOS concentration. This is due to the presence of nanosilica particles within the matrix,

Table 7
Results of thermogravimetric analysis

Sample designation	T_{max} (°C)	Rate of max. degradation (wt% loss/°C) at T_{max}	% Residue at T_{max}
1A85EX	393	1.95	1.30
1A85EN10X	394	2.10	1.89
1A85EN30X	398	1.53	10.73
1A85EN50X	398	1.53	13.36

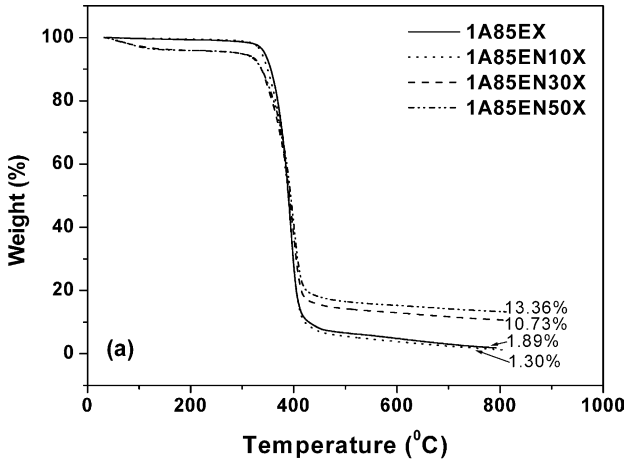

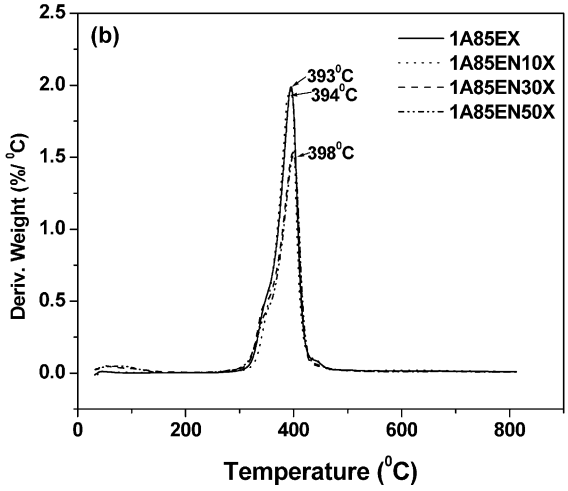

Fig. 10. (a) TGA thermograms of the crosslinked pure and representative hybrid composites; (b) DTG thermograms of the crosslinked pure and representative hybrid composites.

imparting higher stability to the hybrid composites, which increase with increasing nanosilica concentration. The residue also increases with TEOS concentration due to higher silica generation in the hybrid composites.

4. Conclusions

Based on the study performed on the sol–gel hybrid composites comprising of acrylic copolymers/terpolymers having various microstructures and silica, the following conclusions can be drawn.

- Increased polarity of the polymer matrices with different microstructures gives finer dispersion of silica particles (<100 nm) and prevents macrophase separation. Lower polarity causes silica aggregation.
- SEM study shows finer distribution of silica with average particle size of 15 nm in 85EN10, while the 5% acrylic acid modified terpolymer shows finer distribution of silica with an average particle size of 80 nm even at 50 wt% TEOS concentration.
- The mechanical properties increase with increase in polarity of the matrix due to better polymer–silica interaction and uniform nanosilica dispersion. Cross-linking improves the mechanical properties further. The aging resistance of these hybrid nanocomposites is significant.
- Dynamic mechanical properties show reinforcement within the hybrid composites. TEOS loaded samples exhibit higher storage modulus in the rubbery region. Positive shift in T_g ($+25$ °C) and reduction in tan δ_{max} value as well as broadening of the tan δ peak indicates presence of nanosilica interaction. This effect is more prominent in the hybrids with 5% acrylic acid modified terpolymer matrices.
- The nanocomposites show higher thermal stability than the control polymer, which is illustrated by improvement in the rate of degradation and higher T_{max}.

References

[1] Okada A, Usuki A. Mater Sci Eng 1995;C3:109.
[2] Bandyopadhyay A, Bhowmick AK, De Sarkar MD. J Appl Polym Sci 2004;93:2579.
[3] Gilman JW. Appl Clay Sci 1999;15:31.
[4] Messersmith PB, Giannelis EP. J Polym Sci, Part A: Polym Chem 1995;33:1047.
[5] Chen W, Xu Q, Yuan RZ. Compos Sci Technol 2001;61:935.
[6] Godovski DY. Adv Polym Sci 1995;119:79.
[7] Matejka L, Dusek K, Noga J. Wiley Polym Networks Group Rev Ser 1998;1:301.
[8] Matejka L, Dusek K, Plestil J, Lednicky F. Polymer 1998;40:171.
[9] Matejka L, Plestil J, Dusek KJ. Non-Cryst Solids 1998;226:114.
[10] Ring TA. Fundamentals of ceramic powder processing and synthesis. San Deigo: Acadamic Press; 1996.
[11] Kickelbick G. Prog Polym Sci 2003;28:83.
[12] Bandyopadhyay A, De Sarkar M, Bhowmick AK. Rubber Chem Technol 2004;77:830.
[13] Schubert U, Husing N, Lorenz A. Chem Mater 1995;7:2010.
[14] Deng Q, Moore RB, Muritz KA. Chem Mater 1995;7:2261.
[15] Shao PL, Mauritz KA, Moore RB. J Polym Sci, Part B: Polym Phys 1996;34:873.
[16] Chujo Y, Saegusa T. Adv Polym Sci 1992;100:11.
[17] Tamaki R, Chujo Y. Appl Organomet Chem 1998;12:755.
[18] Landry CJT, Coltrain BK, Wesson JA, Zumbulyadis N, Lippert JL. Polymer 1992;33:1496.
[19] Hill DJT, O'Donnell JH, Perera MCS, Pomery PJ. J Polym Sci, Part A: Polym Chem 1996;34:2339.
[20] Martino SDL, Kelchtermans M. J Appl Polym Sci 1995;56:1781.